REMARKS

Claims 10-14, 16-20, 25 and 27-50 were pending in the present application. Claims 11, 25, 30, 33, 38 and 45 have been cancelled without prejudice. New claims 51-54 have been added. The new claims are supported in the claims as originally filed, and at least in the specification at page 8, lines 24-27. Thus, claims 10, 12-14, 16-20, 27-29, 31-32, 34-37, 39-44 and 46-54 are pending.

To further prosecution without acquiescing to the Examiner's arguments, Applicants have amended independent claim 10. As amended, claim 10 relates to a process for preparing randomly-ordered crystal agglomerates comprising an alkali metal clavulanate salt, comprising contacting a solution or suspension of alkali metal clavulanate salt in a solvent or mixture of solvents with one or more anti-solvents under stirring. This amendment is supported in the specification and does not include new matter. (See e.g., specification at page 5, lines 21-28; and at page 7, line 30 through page 8, line 2). Applicants request reconsideration of the Examiner's rejections in the Final Office Action mailed March 10, 2004, maintained in the Advisory Action mailed April 6, 2004, in view of the amended claims.

Rejections under 35 U.S.C. § 102

First, the Examiner rejected claims 37-38, 40-42, and 44-50 under 35 U.S.C. § 102(b), as allegedly being anticipated by U.S. patents 4,454,069; 6,417,352; and 5,288,861. Applicants address the Examiner's rejection in view of the amended claims. As amended, claim 37 relates to an agglomerate of randomly-ordered crystals of an alkali metal clavulanate having a compressibility between about 10 % and 40 %, with the proviso that the rosette-like crystalline form of potassium clavulanate is excluded. Claims 37, 39-44, and 46-50 are not anticipated because U.S. patents 4,454,069; 6,417,352; and 5,288,861 only describe well-defined needles or plates, or rosette forms.

U.S. 5,288,861 ('861) describes potassium clavulanate in rosette form, where a plurality of needle crystals radiate out from a common nucleation point. The '861 patent also teaches that crystalline potassium clavulanate generally exists in the form of rod-like or needle-like crystals.

The crystals are sometimes agglomerated into plate-like crystals, or sometimes randomly aggregated into loosely formed bundles. These forms of potassium clavulanate can give rise to processing difficulties because the material is of low bulk density, and does not always flow readily. ('861, at col. 1, lines 40-48). Contrary to randomly-ordered crystal aggregates, needle crystals by definition, are well-defined structures having a general form. (See e.g., Langer, "Existence of needle crystals in local models of solidification, *Phys. Rev. A* 33: 435-441, attached as Exh. 1). Furthermore, as rosette-like crystalline forms of potassium clavulanates have been excluded in claim 37, this patent does not anticipate the claimed agglomerates.

U.S. patent 4,454,069 ('069) teaches a process for preparing potassium clavulanates as well-defined needles or waisted plates (*i.e.*, butterfly-shaped). ('069, at col. 5, lines 32-39). The clavulanates in the '069 patent were prepared by adding potassium 2-ethyl hexanoate to a solution or suspension of an amine-clavulanate salt.

U.S. patent 6,417,352 ('352) teaches a process for preparing potassium clavulanates that is similar to the '069 patent, where potassium-2-ethyl hexanoate is added to clavulanic acid, instead of an amine-clavulanate salt. As indicated at column 4, lines 40-56, "conversion from sodium clavulanate to potassium clavulanate is carried out by extraction of clavulanic acid to an adequate solvent and crystallization of potassium clavulanate after dilution of the acid . . . and addition of potassium 2-ethylhexanoate or potassium acetate solution." Although the '352 patent does not specify the form of potassium clavulanates, conditions which would be expected to obtain needles forms were used. Because the '861, '069 or '352 patent do not teach aggregates of randomly-ordered crystals of an alkali metal clavulanate salt, claims 37, 39-44, and 46-50 are not anticipated. Applicants therefore, respectfully request that this rejection be withdrawn.

Second, the Examiner rejected claims 37-50 under 35 U.S.C. § 102(b), as allegedly being anticipated by WO 97/33564. Claims 37, 39-44, and 46-50 are not anticipated because WO 97/33564 only describe agglomerates of penicillin V potassium, phenoxymethylpenicillin potassium, amoxicillin trihydrate, and cephalexin monohydrate. While these antibiotic agglomerates may be mixed with a second pharmaceutically active agent such as potassium

clavulanate, the potassium clavulanate itself is not an agglomerate of randomly-ordered crystals. Thus, WO 97/33564 does not anticipate claims 37, 39-44 and 46-50, and Applicants respectfully request that this rejection be withdrawn.

Third, the Examiner rejected claims 10-14, 16-19, 27, 27-32, 37-38 and 42-45 under 35 U.S.C. § 102(b), as allegedly being anticipated by WO 98/21212. Claims 37, 39-44, and 46-50 are not anticipated because WO 98/21212 only describes rosette or needle formed crystals, or a cluster of needle formed crystals (WO 98/21212, at page 4, lines 17-18). As previously indicated, needles have well-defined structures, unlike the randomly-ordered crystal clusters of the claimed invention. Thus, WO 98/21212 does not anticipate claims 37, 39-44 and 46-50, and Applicants respectfully request that this rejection be withdrawn.

Furthermore, the needles obtained using the process taught in WO 98/21212 have a compressibility of about 50 %, as shown in Table 1 (Specification at Example 8). In the Advisory Action, the Examiner indicated that "[t]here is no way of knowing where this needle material came from." (Advisory Action, page 3). Contrary to the Examiner's assertions, the needles were prepared using conditions that are similar to those described in Example 6 of WO 98/21212. In particular, needles of potassium clavulanate were prepared by suspending diclavulanate salt of bis(2-dimethylaminoethyl) ether in acetone and water. Under stirring, a solution of potassium 2-ethylhexanoate in acetone was added. (See, specification at page 17, lines 4-10).

WO 98/21212 also fails to teach a process for preparing crystallized agglomerates comprising an alkali metal clavulanate salt, comprising contacting an alkali metal clavulanate salt in a solvent or mixture of solvents with one or more anti-solvents under stirring. In contrast, WO 98/21212 teaches a process where a potassium source in a solvent, is added to a amine salt in a solvent, preferably in a water miscible ketone or alcohol. In a particular example, potassium 2-ethylhexanoate in acetone was added to bis(2-(dimethylamino)ethyl) ether diclavulanate in a mixture of acetone and water. In the Advisory Action, the Examiner indicated that "[t]he exact instant the K salt is formed in that solution, it will meet the claim language requirement of

potassium clavulanate, and at that point, the solvent limitation is met as well." (Advisory Action, pages 2-3).

Contrary to the Examiner's assertions, the formation of potassium salt in solution alone does not meet the claim language, because the potassium clavulanate solution is not contacted with another portion of anti-solvent. On the other hand, agglomerates of randomly-ordered clusters of alkali metal clavulanate salts may be prepared, for example, by adding a solution of potassium clavulanate in a mixture of water/acetone to acetone. (See e.g., specification at Example 1). Furthermore, as previously indicated, the potassium clavulanates obtained using the process taught in WO 98/21212 are rosette or needle formed crystals, or a cluster of needle formed crystals. Because WO 98/21212 fails to teach agglomerates of randomly-ordered clusters of an alkali metal clavulanate salt, or a process of preparing such agglomerates, claims 10, 12-14, 16-20, 27-29, 31-32, 34-37, 39-44 and 46-50 are not anticipated. Applicants therefore, respectfully request that this rejection be withdrawn.

Further, new claims 51-54 are not anticipated by the prior art references cited by the Examiner. Specifically, claims 51-52 are dependent on claim 37, and contain all the limitations in claim 37. Claim 53-54 are dependent on claim 10, and contain all the limitations in claim 10. As previously discussed, claims 10 or 37 are not anticipated. Accordingly, claims 51-54 are not anticipated.

Rejection under 35 U.S.C. § 112, second paragraph

The Examiner rejected claims 31 and 45 under 35 U.S.C. § 112, as allegedly being indefinite, for reciting "compressibility" (claim 31) and "flowability" (claim 45). Claim 45 has been canceled without prejudice, rendering this rejection moot.

Regarding "compressibility," Applicants have amended the claims to recite "Carr index compressibility." The recitation of the term "Carr index" merely includes art-recognized definitions known at the time of filing the application, and is not considered new matter. See MPEP § 2163.07. As commonly known in the art, Carr's index is the percentage calculated as 100 times the ratio of

the difference between tapped bulk density and loose bulk density to the tapped bulk density. (See e.g., Gohel *et al.*, "Development and evaluation of a multifunctional directly compressible diluent consisting of brittle and ductile materials," Pharm. Tech., December 4, 2003, attached as Exh. 2). The Carr index was also used for calculating compressibility in the Examples. As amended, the claims are definite, and Applicants respectfully request that this rejection be withdrawn.

Rejections under 35 U.S.C. § 112, first paragraph

The Examiner rejected claims 10-14, 16-20, 25, 27-32, 35-45 and 47-50 under 35 U.S.C. § 112, first paragraph, as allegedly failing to comply with the enablement requirement. As amended, the claims relate to agglomerates comprising an alkali metal clavulanate salt, and processes of preparing such agglomerates. In the Advisory Action, the Examiner indicated that such an amendment, if entered, would result in enabled claims. Thus, Applicants respectfully request that this rejection be withdrawn.

Furthermore, the Examiner rejected claims 10-14, 16-20, 25 and 27-50 under 35 U.S.C. § 112, first paragraph, as allegedly failing to comply with the written description requirement. The Examiner alleged that the removal of a previous limitation of "high water affinity" results in compounds beyond what the specification teaches. (Final Office Action, page 6). The Examiner also alleged that the removal of the previous limitation of "high water affinity" has broadened the claims. Applicants must respectfully disagree. While the previous limitation of "high water affinity" has been removed, the amended claims relate specifically to agglomerates of randomly-ordered clusters of an alkali metal clavulanate salt, and processes of preparing such compounds. The amended claims reasonably convey to one skilled in the art that the inventor(s) had possession of the claimed invention at the time the application was filed. Thus, Applicants respectfully request that this rejection be withdrawn.

In view of the above, each of the presently pending claims in this application is believed to be in immediate condition for allowance. Accordingly, the Examiner is respectfully requested to withdraw the outstanding rejection of the claims and to pass this application to issue. If it is

determined that a telephone conference would expedite the prosecution of this application, the Examiner is invited to telephone the undersigned at the number given below.

In the event the U.S. Patent and Trademark office determines that an extension and/or other relief is required, applicant petitions for any required relief including extensions of time and authorizes the Commissioner to charge the cost of such petitions and/or other fees due in connection with the filing of this document to Deposit Account No. 03-1952 referencing docket no. 246152015000. However, the Commissioner is not authorized to charge the cost of the issue fee to the Deposit Account.

Dated: May 6, 2004

Respectfully submitted,

By 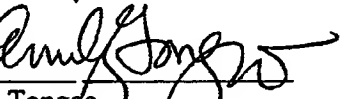

Emily C. Tongoo
Registration No.: 46,473
MORRISON & FOERSTER LLP
3811 Valley Centre Drive, Suite 500
San Diego, California 92130
(858) 314-5413

BEST AVAILABLE IMAGES

Defective images within this document are accurate representations of the original documents submitted by the applicant.

Defects in the images may include (but are not limited to):

- BLACK BORDERS
- TEXT CUT OFF AT TOP, BOTTOM OR SIDES
- FADED TEXT
- ILLEGIBLE TEXT
- SKEWED/SLANTED IMAGES
- COLORED PHOTOS
- BLACK OR VERY BLACK AND WHITE DARK PHOTOS
- GRAY SCALE DOCUMENTS

IMAGES ARE BEST AVAILABLE COPY.

As rescanning documents *will not* correct images, please do not report the images to the Image Problem Mailbox.

PHYSICAL REVIEW A VOLUME 33, NUMBER 1 JANUARY 1986

Existence of needle crystals in local models of solidification

J. S. Langer
Institute for Theoretical Physics, University of California, Santa Barbara, California 93106
(Received 31 July 1985)

The way in which surface tension acts as a singular perturbation to destroy the continuous family of needle-crystal solutions of the steady-state growth equations is analyzed in detail for two local models of solidification. All calculations are performed in the limit of small surface tension or, equivalently, small velocity. The basic mathematical ideas are introduced in connection with a quasilinear, isotropic version of the geometrical model of Brower *et al.*, in which case the continuous family of solutions disappears completely. The formalism is then applied to a simplified boundary-layer model with an anisotropic kinetic attachment coefficient. In the latter case, the solvability condition for the existence of needle crystals can be satisfied whenever the coefficient of anisotropy is arbitrarily small but nonzero.

I. INTRODUCTION

There is growing evidence that pattern selection in local models of dendritic solidification is closely connected with the existence of so-called "needle-crystal" solutions of the steady-state equations of motion. In both the geometrical[1,2] and boundary-layer[3,4] models that have been introduced recently, as well as in more realistic nonlocal models of solidification with diffusion control,[5] there exists a continuous family of "Ivantsov"[6,7] needle crystals when surface tension is omitted. The addition of surface tension, however, is a singular perturbation of these systems which, at least in the local versions—that is, the geometrical and boundary-layer models—destroys the family of solutions and opens the possibility that sharp selection of growth rates, tip radii, etc., occurs via a solvability condition. It seems possible that a similar phenomenon occurs in the fully nonlocal problem.

The purpose of the present paper is to examine in some detail the breakdown of the Ivantsov solutions in both of the local models. The way in which this breakdown occurs provides some interesting clues about the roles played by surface tension and crystalline anisotropy in the dendrite theory. Moreover, this singular perturbation problem is of mathematical interest in its own right. As we shall see, the method of solution proposed here seems reasonable but is not rigorous or even systematic. It can, however, be tested by direct numerical computations; and the results of such tests make it plausible that the analytic approximation captures the essential features of the relevant phenomena. Indeed, as this paper is being written, it appears that there may be important new progress both in understanding the mathematical nature of the problem as posed here[8] and in showing that the basic features of this model problem also appear in the more realistic systems.[9–11] This paper has therefore been organized to serve as a starting point for study of these later developments.

We shall begin in Sec. II by looking at the simplest nontrivial version of the geometrical model in order to describe the mathematical strategy with a minimum of unnecessary complication. That strategy will be outlined in Sec. III. In Sec. IV we shall apply this method to a minimal version of the boundary-layer model, and shall see there how crystalline anisotropy may play an essential role in the selection of needle-crystal solutions. Some mathematical and computational details pertaining to both models are relegated to an appendix.

II. THE QUASILINEAR GEOMETRICAL MODEL

In all of the following, we shall restrict our attention to two-dimensional local models in which a moving one-dimensional interface is described by specifying its curvature $K=\partial\theta/\partial s$ as a function of arc length s. The relevant geometry is illustrated in Fig. 1. The basic assumption of the geometrical models[1,2] is that v_n, the normal velocity of the interface, is a function only of K and its even derivatives with respect to s. The steady-state condition is simply

$$v_n(K,d^2K/ds^2,\ldots)=v\cos\theta\,, \tag{2.1}$$

so that the interface is moving at constant velocity v, without change in its shape, in a fixed direction. A needle crystal, by definition, is a solution of (2.1) that has the general form shown in Fig. 1 in which

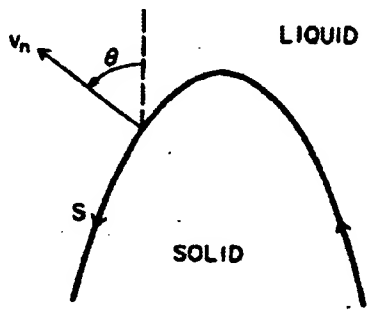

FIG. 1. Geometry of the needle crystal.

$$K\to 0,\quad \theta\to\pm\pi/2 \quad \text{as } s\to\pm\infty\ . \tag{2.2}$$

The analog of the Ivantsov limit in the geometrical model occurs when we set v_n to be a function of K alone. If (2.1) is piecewise invertible for K as a function of θ, then $K(\theta)=d\theta/ds$ is a first-order ordinary differential equation which generally is solvable for θ as a function of s. We may further expect that these solutions will satisfy the needle-crystal conditions (2.2) for some continuous range of values of the parameter v. For example, the simplest possible choice is $v_n=K$, for which it turns out that

$$\theta=\cos^{-1}(\operatorname{sech} vs)\ , \tag{2.3}$$

a relation which satisfies (2.2) for all v. The family of Ivantsov solutions is conventionally characterized by the relation between v and the tip radius $R=K^{-1}(\theta=0)$, which in this case is trivially $Rv=1$.

The above solutions are all strongly unstable. In fact, the model as it stands is not even dynamically well defined because the amplification rate of deformations is unbounded at short wavelengths. In order to produce a model whose time dependence is meaningful, it is necessary to add a term which mimics the effect of surface tension and stabilizes the system at short wavelengths. The easiest way to do this is to write

$$v_n=K+\gamma^2\frac{d^2K}{ds^2}\ , \tag{2.4}$$

where γ plays the role of a capillary length. Equation (2.4) defines what might be called a quasilinear geometrical model; the right-hand side is linear in K. This model does not actually produce dendrites, but its dynamical behavior is well defined and quite interesting in some respects.

Our aim now is to see what effect the second derivative in (2.4) has on the needle-crystal solutions (2.3). To do this, it is convenient first to rewrite the steady-state equation (2.1) in the form

$$\kappa=\cos\theta-\nu\frac{d^2\kappa}{d\xi^2}\ , \tag{2.5}$$

where $\nu=(\gamma v)^2$, $K=v\kappa$, and $\xi=vs$. Equivalently,

$$\kappa=\cos\theta-\frac{\nu}{2}\kappa\frac{d^2\kappa^2}{d\theta^2}\ . \tag{2.6}$$

The latter form, in which ξ has been replaced by θ as the independent variable by using $\kappa=d\theta/d\xi$, is very useful but can produce spurious difficulties unless κ is everywhere non-negative.

Equations (2.5) and (2.6) can be used to illustrate some points that have been made in previous papers.[2,3] If we iterate the right-hand side of (2.6), we generate a series expansion for κ in powers of ν and $\cos\theta$. Each term in this series is consistent with the needle-crystal conditions (2.2), and the series appears to produce an accurate estimate for κ especially far down the needle where $\cos\theta$ is small. However, we know that this series can be at best asymptotic. To see this, write (2.5) as a set of three coupled equations for a ξ-dependent trajectory in the space of variables θ, $\kappa=d\theta/d\xi$, and $\lambda=d\kappa/d\xi$. As has been noted previously,[2] only one trajectory emerges from the fixed point at $\theta=-\pi/2$, $\kappa=\lambda=0$; similarly, only one trajectory enters the reflected fixed point at $\theta=+\pi/2$. For a needle crystal to exist, these two pieces must belong to a single trajectory which joins the fixed points and, by symmetry, passes through some point on the κ axis with $\theta=\lambda=0$. There is no special reason for this to happen. In general, the trajectories entering or leaving the fixed points, even if well approximated by some finite number of terms of the above series in powers of ν, need not reach $\theta=0$—the tip of the needle—with $\lambda=d\kappa/d\xi=0$. Our goal in what follows is to compute λ at $\theta=0$ explicitly and to discover under what conditions it might vanish.

As we shall see immediately, the mathematical problem posed above is highly nontrivial. To make some progress analytically, we shall look only at small values of ν; that is, we shall look in the neighborhood of the known solution of (2.6), $\kappa_0(\theta)=\cos\theta$ at $\nu=0$. We then shall consider solutions of (2.6) for nonzero ν that satisfy the needle-crystal conditions (2.1) for $\theta\to+\pi/2$, and shall examine their behavior near $\theta=0$. This strategy is based on the assumption that, if ν is sufficiently small, the difference between κ and κ_0 also will be small in the interval $0\le\theta\le\pi/2$ and may be computable by a linear approximation. For arbitrary ν, the continuation of this solution to negative θ may not remain small or even well defined, but the latter behavior need not invalidate an approximation in the region of interest. The trouble with this procedure turns out to be that $\lambda(\theta=0)$ vanishes more rapidly than any finite power of ν. Indeed, a systematic expansion in powers of ν must necessarily recover just the asymptotic series described above for which $\lambda(0)$ vanishes identically term by term. As a result, any useful scheme of approximation must go beyond a simple series in powers of the small parameter ν.

To examine this situation in greater detail, define

$$\kappa-\cos\theta\equiv\nu\kappa_1\ , \tag{2.7}$$

and write (2.6) in the form

$$\nu\frac{d^2\kappa_1}{d\theta^2}-2\nu\tan\theta\frac{d\kappa_1}{d\theta}+\frac{1}{\cos^2\theta}[1+\nu(1-3\cos^2\theta)]\kappa_1 = -\frac{1}{\cos\theta}(1-2\cos^2\theta)+\mathcal{N}(\kappa_1)\ , \tag{2.8}$$

where $\mathcal{N}(\kappa_1)$ is a nonlinear term of orders $\nu^2\kappa_1^2$ and $\nu^3\kappa_1^3$ containing at most two differentiations of these quantities with respect to θ. The structure of (2.8) suggests that each differentiation with respect to θ produces a factor $1/\sqrt{\nu}$. We shall see this explicitly in what follows. Thus, a systematic approximation for (2.8) might involve dropping $\mathcal{N}$ and the term proportional to ν in square brackets on the left-hand side, or perhaps treating these terms perturbatively. The term containing $\nu d\kappa_1/d\theta$, which is formally of order $\sqrt{\nu}$, turns out to be essential. In Sec. III we shall examine the consequences of the above approximation. It will be useful to describe the calculation in general terms so that the technique may be applied to the boundary-layer model in Sec. IV without repetitive explanations.

III. APPROXIMATION SCHEME

The general structure of (2.8), with or without the terms to be omitted, is

$$\nu\frac{d^2\kappa_1}{d\theta^2}+\nu p(\theta)\frac{d\kappa_1}{d\theta}+q(\theta)\kappa_1=r(\theta)\ . \tag{3.1}$$

The range of θ is $[0,\pi/2]$. Boundary conditions are to be imposed only at $\theta=\pi/2$. These are the needle-crystal conditions (2.2) which require that κ and $\lambda=d\kappa/d\xi=\kappa\, d\kappa/d\theta$ vanish as $\xi\to\infty$, $\theta\to\pi/2$. If we are working only to first order in κ_1, then this condition requires that κ_1 and $\kappa_0 d\kappa_1/d\theta$ vanish at $\pi/2$, where κ_0 denotes the Ivantsov solution; that is, $\kappa_0=\cos\theta$ for the geometrical model. Another way of stating this is that we want κ_1 to be consistent near $\pi/2$ with the asymptotic expansion of κ in powers of ν and $\cos\theta$. To lowest order in ν, this means

$$\kappa_1\simeq r_0(\theta)/q_0(\theta),\quad \theta\to\pi/2 \tag{3.2}$$

where r_0 and q_0 are the values of r and q at $\nu=0$. Finally, the problem that we pose for ourselves is to compute $\lambda=d\kappa/d\xi$, or simply $d\kappa/d\theta$, at $\theta=0$.

For sufficiently small ν, (3.1) can be solved by a Wentzel-Kramers-Brillouin (WKB) approximation. The homogeneous solutions are

$$\kappa_\pm^{\rm hom}(\theta)\simeq\frac{1}{q_0^{1/4}}\exp\left[\pm\frac{i}{\sqrt{\nu}}\psi(\theta)-\tfrac{1}{2}\int_0^\theta p_0(\phi)d\phi\right], \tag{3.3}$$

where

$$\psi(\theta)=\int_0^\theta q_0^{1/2}(\phi)d\phi\ , \tag{3.4}$$

and we have neglected terms of order $\sqrt{\nu}$ or smaller in the exponent and in the prefactor. These solutions should be accurate as long as

$$\left|\frac{1}{q_0}\frac{dq_0}{d\theta}\right|\ll\left|\frac{q_0}{\nu}\right|^{1/2}, \tag{3.5}$$

for all θ in $[0,\pi/2]$.

For the quasilinear geometrical model, $q_0=(\cos\theta)^{-2}$, and (3.5) is satisfied for $\nu\ll 1$. Moreover, $\psi(\theta)$ in (3.4) is equal to the unperturbed dimensionless arc length ξ obtained from $\kappa_0=d\theta/d\xi=\cos\theta$. Using $p_0=-2\tan\theta$, we find

$$\kappa_\pm^{\rm hom}(\theta)\simeq\frac{1}{(\cos\theta)^{1/2}}\exp\left[\pm\frac{i}{\sqrt{\nu}}\ln\left|\frac{1+\sin\theta}{\cos\theta}\right|\right]$$
$$=(\cosh\xi)^{1/2}\exp\left[\pm\frac{i\xi}{\sqrt{\nu}}\right]. \tag{3.6}$$

For small ν, these are rapidly oscillating functions whose amplitudes diverge as $\theta\to\pi/2$, $\xi\to\infty$. Equation (3.6) is an analytic statement of the fact that only one trajectory in θ,κ,λ space enters the fixed point at $\theta=\pi/2$, $\kappa=\lambda=0$, and all other trajectories spiral out and away from that point. It also justifies our expectation that differentiations in (2.8) produce factors of $1/\sqrt{\nu}$.

The next step is to use the homogeneous solutions (3.3) to compute a particular solution of (3.1) by means of the formula

$$\kappa_1^{\rm part}(\theta)=\frac{1}{\nu}\int^\theta d\phi\frac{r(\phi)}{W(\phi)}\left[\kappa_+^{\rm hom}(\theta)\kappa_-^{\rm hom}(\phi)-\kappa_-^{\rm hom}(\theta)\kappa_+^{\rm hom}(\phi)\right], \tag{3.7}$$

where the Wronskian W is

$$W=\kappa_-^{\rm hom}\frac{d\kappa_+^{\rm hom}}{d\phi}-\kappa_+^{\rm hom}\frac{d\kappa_-^{\rm hom}}{d\phi}\ . \tag{3.8}$$

The lower limit of integration remains to be chosen. Because both of the homogeneous solutions $\kappa_\pm^{\rm hom}(\theta)$ which appear in (3.7) are inconsistent with the needle-crystal conditions, the only possible choice for this lower limit is $\pi/2$. Using (3.3), we find

$$W(\theta)\simeq\frac{2i}{\sqrt{\nu}}\exp\left[-\int_0^\theta p\,d\phi\right], \tag{3.9}$$

and

$$\kappa_1(\theta)\simeq-\frac{1}{\sqrt{\nu}}\int_\theta^{\pi/2}d\phi\frac{r_0(\phi)}{[q_0(\theta)q_0(\phi)]^{1/4}}\times\exp\left[-\tfrac{1}{2}\int_\phi^\theta p_0\,d\phi'\right]\times\sin\{(1/\sqrt{\nu})[\psi(\theta)-\psi(\phi)]\}\ . \tag{3.10}$$

To check that (3.10) does satisfy the asymptotic condition (3.2), integrate (3.10) twice by parts, integrating the sine as if to obtain a series in growing powers of ν. The result is

$$\kappa_1(\theta)\approx\frac{r_0(\theta)}{q_0(\theta)}+\nu M(\theta)+\cdots\ , \tag{3.11}$$

where M is a function of θ which is of no special interest except for the fact that it exists and is well behaved near $\theta=\pi/2$.

Our goal is to calculate $d\kappa/d\theta$ at $\theta=0$, which we denote by the symbol $\kappa'(0)$. Note that the symmetry of the system requires that q and r be even functions of θ and that p be odd. Thus

$$\kappa'(0)=-\tfrac{1}{2}[q_0(0)]^{1/4}\int_{-\pi/2}^{\pi/2}d\theta\frac{r_0(\theta)}{[q_0(\theta)]^{1/4}}\times\exp\left[\tfrac{1}{2}\int_0^\theta p\,d\phi\right]\times\cos\left[\frac{\psi(\theta)}{\sqrt{\nu}}\right]. \tag{3.12}$$

Equation (3.12) is the principal result whose validity and implications are to be explored in the remainder of this paper.

Remember that the condition for existence of a needle crystal is that $\kappa'(0)$ vanish. It is interesting, and possibly useful for future analysis, to note that (3.12) with $\kappa'(0)=0$ can be interpreted as a solvability condition for the (formally) linear inhomogeneous equation (3.1). To see this, consider (3.1) in the whole interval $[-\pi/2,+\pi/2]$ and

look for solutions in the space of symmetric functions $\kappa_1(\theta)$. The function

$$\kappa_{\rm sym}^{\rm hom}(\theta)=\frac{1}{q_0^{1/4}}\exp\left[-\tfrac{1}{2}\int_0^\theta p\,d\phi\right]\cos\left[\frac{\psi(\theta)}{\sqrt{\nu}}\right] \quad (3.13)$$

is the WKB approximation for the solution of $\mathcal{L}\kappa=0$, where $\mathcal{L}$ denotes the linear operator on the left-hand side of (3.1), and

$$\tilde{\kappa}_{\rm sym}^{\rm hom}(\theta)=\frac{1}{W(\theta)}\kappa_{\rm sym}^{\rm hom}(\theta)$$

$$\simeq\frac{2i}{\sqrt{\nu}}\frac{1}{q_0^{1/4}}\exp\left[\tfrac{1}{2}\int_0^\theta p\,d\phi\right]\cos\left[\frac{\psi(\theta)}{\sqrt{\nu}}\right] \quad (3.14)$$

is the solution of the adjoint equation $\tilde{\mathcal{L}}\tilde{\kappa}=0$. Thus, the solvability condition derived above has the form

$$\int_{-\pi/2}^{\pi/2}d\theta\, r(\theta)\tilde{\kappa}_{\rm sym}^{\rm hom}(\theta)=0\,, \quad (3.15)$$

which is the usual statement that the inhomogeneous term $r(\theta)$ can have no projection onto the null space of $\mathcal{L}$ if (3.1) is to have a solution. One obscure aspect of this interpretation is the definition of the function space; the divergent functions $\kappa^{\rm hom}(\theta)$ would not seem to belong to the space of acceptable needle-crystal solutions. One can make this difficulty seem less severe by working with the bounded functions $W^{-1/2}\kappa$; that is, by transforming away the first derivative in (3.1). But this mathematical point, among many such points raised in this paper, requires further scrutiny.

The general character of (3.12) can be seen by evaluating it for the quasilinear geometrical model where $q_0=(\cos\theta)^{-2}$, $p_0=-2\tan\theta$, $r_0=(2\cos^2\theta-1)/\cos\theta$, $\psi=\xi$, and $\cos\theta=\operatorname{sech}\xi$. Then, transforming to ξ as the variable of integration, we find

$$\kappa'(0)\simeq-\tfrac{1}{2}\int_{-\infty}^{\infty}d\xi(\operatorname{sech}^{3/2}\xi)(2\operatorname{sech}^2\xi-1)e^{i\xi/\sqrt{\nu}}$$

$$\approx-\frac{A}{\nu^{3/4}}\exp\left[-\frac{\pi}{2\sqrt{\nu}}\right], \quad (3.16)$$

where

$$A=\frac{16\sqrt{\pi}}{15}\simeq1.8906\,. \quad (3.17)$$

The derivation of the second form of (3.16), valid in the limit $\nu\ll1$, is summarized in the Appendix. The important point to notice is that (3.16) has an essential singularity at $\nu=0$, consistent with the failure of expansions in powers of ν.

A comparison between (3.16) and a direct numerical integration of the fully nonlinear equation (2.5) confirms the basic form of (3.16), both the exponential function and the power of ν in the prefactor. The numerically determined value of A, however, appears to be about 3.7 ± 0.2, larger than that given by (3.17) by a factor of about 2. This comparison was made for values of ν in the interval $0.002\le\nu\le0.01$, across which $\kappa'(0)$ changes by eight decades. The validity of the asymptotic evaluation of the integral in (3.16) was also checked in this interval by direct numerical integration, thus confirming that these values of ν are small enough to be in the asymptotic region.

The source of this discrepancy is related to the fact that the power of ν in the prefactor in (3.16), i.e., $\nu^{-3/4}$, is determined by the highest power of $\operatorname{sech}\xi$ in the integrand, which in turn can be traced back to the highest power of $\cos\phi$ in $r_0(\phi)$ in (3.10). (This will be seen explicitly in the Appendix, but should be apparent from (3.16) because there we are computing the high-frequency—small-ν—behavior of a Fourier transform.) Now think about a first nonlinear correction to r. That is, consider using the approximation for κ_1 given in (3.10) to evaluate $\mathcal{N}(\kappa_1)$ and including the result in r on the right-hand side of (3.1). The resulting corrections to r will be formally of relatively high order in ν but will contain various powers of $\cos\theta$, and the latter will produce inverse powers of ν in the final expression for $\kappa'(0)$. The exponential part of (3.16) will be unchanged by this procedure, but apparently the prefactor is not being computed systematically.

This line of analysis will not be pursued further in this paper. It appears that there may be a much more elegant and mathematically controlled way of arriving at formulas such as (3.16).[8] The interested reader—along with the author—should be alert for new developments in this class of problems.

IV. THE MINIMAL BOUNDARY-LAYER MODEL

The boundary-layer model[3,4] has been introduced as an attempt to include in a local description some physical features of the real solidification problem that are missing in the purely geometrical approach. In particular, the dynamics of a thermal boundary-layer field defined along the solidification front mimic some of the nonlocality and history dependence associated with a more realistic thermal diffusion field. The model has had some successes. Its steady-state solutions, including the parabolic needle crystal in the Ivantsov limit, are nearly identical to those of the full model. The boundary-layer model does produce time-dependent dendritic patterns whose growth rates and tip radii are numerically consistent with solvability conditions for needle crystals with nonvanishing surface tension. At present, however, it is still not known whether the model produces a physically realistic picture of dendritic sidebranching.

In order to make the following analysis reasonably tractable, we shall consider only a minimal version of the boundary-layer model in which the dimensionless undercooling Δ becomes vanishingly small. This is not the physically most realistic limit of the model, but it retains most of the features which seem essential for present purposes. (The opposite limit, $\Delta\to1$, will be discussed elsewhere.) The steady-state equation to be considered is the same as that of Ref. (3), Eq. (5.17), supplemented by an anisotropic kinetic attachment coefficient. Specifically,

$$\kappa=\cos^3\theta-\nu\kappa\cos^2\theta\frac{d}{d\theta}\left[\frac{\kappa}{\cos\theta}\frac{d}{d\theta}(\kappa+b_m\cos\theta)\right], \quad (4.1)$$

where the κ in Ref. 3 has been replaced by $\nu\kappa$ in order to emphasize the analogy to (2.6). Here, $\nu = d_0 v / D\Delta^5$, where d_0 is a capillary length proportional to surface tension, D is the diffusion constant in the liquid, and v is the growth velocity as before. Note that, as in the geometrical model, ν vanishes in the limit of vanishing surface tension and velocity. The quantity b_m in (4.1) is the θ-dependent kinetic coefficient. In the notation of Ref. 4, $b_m = a\Delta^2(1-\cos m\theta)$. From here on, we shall specialize to the case $m=4$, and write $b_4 = 8\beta_4 \cos^2\theta \sin^2\theta$.

The Ivantsov limit of (4.1), $\kappa_0(\theta) = \cos^3\theta$ is a parabola which has unit radius of curvature at its tip and which trivially satisfies the needle-crystal conditions (2.2) for all ν. In analogy to (2.7), let

$$\kappa - \cos^3\theta \equiv \nu\kappa_1 , \tag{4.2}$$

and rewrite (4.1) in terms of κ_1. The result is an equation of the form (3.1) with

$$p_0(\theta) = -5\tan\theta + \frac{8\beta_4}{\cos^3\theta}\frac{d}{d\theta}(\cos^3\theta \sin^2\theta) , \tag{4.3}$$

$$q_0(\theta) = \frac{1}{\cos^7\theta} , \tag{4.4}$$

$$r_0(\theta) = 3\cos\theta(5\cos^2 - 4) - \frac{8\beta_4}{\cos^2\theta}\frac{d}{d\theta}\left[\cos^2\frac{d}{d\theta}(\cos^3\theta\sin^2\theta)\right] . \tag{4.5}$$

Inserting these functions into (3.12), we obtain

$$\kappa'(0) \simeq -\tfrac{1}{2}\int_{-\infty}^{\infty} d\psi\, r_0(\theta)(\cos\theta)^{\lambda} \times \exp(10\beta_4 \sin^2\theta) e^{i\psi/\sqrt{\nu}} , \tag{4.6}$$

where $\lambda = \frac{31}{4} + 12\beta_4$ and

$$\psi(\theta) = \int_0^{\theta} d\phi \frac{1}{\cos^{7/2}\phi} . \tag{4.7}$$

Notice that, in contrast to the geometrical model (3.16), ψ in (4.7) is not quite the same as the unperturbed arc length ξ defined by

$$\xi(\theta) = \int_0^{\theta} d\phi \frac{1}{\kappa_0(\phi)} = \int_0^{\theta} d\phi \frac{1}{\cos^3\phi} . \tag{4.8}$$

The integral on the right-hand side of (4.6) can be evaluated asymptotically in the limit of small ν. Look, for the moment, at the case $\beta_4 = 0$, so that the only integrals needed are Fourier transforms of powers of the function $\cos\theta(\psi)$. An analysis which is outlined in the Appendix yields the estimate

$$\int_{-\infty}^{\infty} d\psi (\cos\theta)^{\mu} e^{i\psi/\sqrt{\nu}} \simeq C(\mu)\nu^{-\alpha}\exp(-a_s/\sqrt{\nu}) , \tag{4.9}$$

where

$$a_s = \int_0^1 (1-u^2)^{3/4} du = \tfrac{3}{5}\sqrt{2/\pi}[\Gamma(\tfrac{1}{4})]^2 = 0.7189\ldots , \tag{4.10}$$

$$\alpha = \frac{\mu}{7} - \frac{1}{2} , \tag{4.11}$$

and

$$C(\mu) = (\tfrac{2}{7})^{2\mu/7}\frac{2\pi}{\Gamma(2\mu/7)} . \tag{4.12}$$

As in (3.16), the dominant exponential in (4.9) is independent of μ, but the power of ν^{-1} in the prefactor increases with increasing μ. For $\beta_4 = 0$, the leading μ is $\frac{43}{4}$, and

$$\kappa'(0) \simeq -\frac{B}{\nu^{29/28}}\exp\left[-\frac{0.7189}{\sqrt{\nu}}\right] , \tag{4.13}$$

with

$$B = \tfrac{15}{2}C(\tfrac{43}{4}) \simeq 0.4703 . \tag{4.14}$$

Both numerical evaluation of the integral in (4.6) and numerical integration of the fully nonlinear differential equation (4.1) confirm the general form of (4.13). Specifically, a graph of

$$-2\nu^{3/2}\frac{d}{dv}\ln[-\kappa'(0)] \simeq a - 2a\sqrt{\nu} + \cdots \tag{4.15}$$

versus $\sqrt{\nu}$, evaluated for $0.0015 \le \nu \le 0.01$ and extrapolated to small $\sqrt{\nu}$, yields $a = 0.71 \pm 0.02 \simeq a_s$ and a value of α of about unity, consistent with $\frac{29}{28}$. A value of B of about 0.8 fits the integration of (4.1), whereas numerical evaluation of the approximation (4.6) confirms (4.14) in giving a value of B of about 0.5. The latter discrepancy is in the same sense and of about the same size as that which occurred for the geometrical model.

The idea that the dominant behavior of $\kappa'(0)$ at small ν is determined by the highest power of $\cos\theta$ in (4.6) provides some interesting information about the effect of crystalline anisotropy. When the anisotropy coefficient β_4 is nonzero, the dominant θ dependence in $r_0(\theta)$ comes from the second term on the right-hand side of (4.5) and enters with the opposite sign. That is, the leading term in $r_0(\theta)$ is proportional to $-\beta_4\cos^5\theta$ instead of $+\cos^3\theta$. As a result, $\kappa'(0)$ must be positive as ν approaches zero. At larger values of ν, however, the exponential factor in (4.6) is no longer oscillating so rapidly, the slower variations in $r_0(\theta)$ make the dominant contributions, and $\kappa'(0)$ becomes negative again. The situation is illustrated in Fig. 2 where $\kappa'(0)$ is drawn as a function of ν for $\beta_4 = 0$, 0.1, and 0.2. These graphs extend out to $\nu = 0.1$, well beyond the asymptotic regime, and have been obtained by integrating the fully nonlinear equation (4.1). Equation (4.6) does seem to remain a qualitatively good approximation as shown by the dashed curves in the figure.

The important point is that, for $\beta_4 \neq 0$, $\kappa'(0)$ vanishes at a finite value of ν, indicating the existence of a steady-state needle crystal. For this particular version of the model, that is, the minimal boundary-layer model ($\Delta \to 0$) with the special form of kinetic anisotropy indicated in (4.1), such steady-state solutions occur at arbitrarily small but nonzero values of the anisotropy coefficient β_4. However, the selected value of $\nu = d_0 v / D\Delta^5$ becomes small as β_4 decreases, and it seems highly unlikely that needle crystals with very small v or, equivalently, small d_0 can be stable. Thus, it seems that the minimum value of β_4 required for dendritic behavior in this model is nonzero and is determined by a stability requirement.

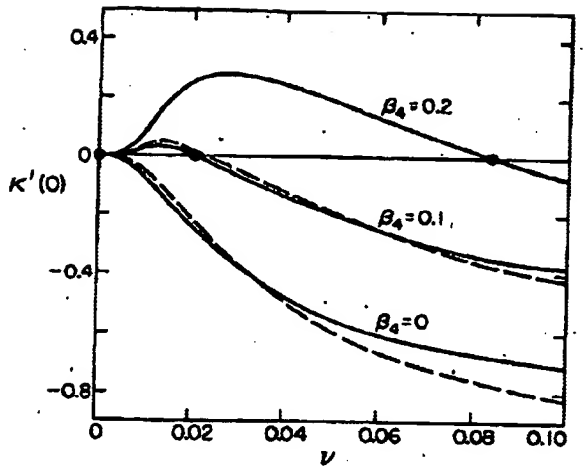

FIG. 2. $\kappa'(0)$ as a function of ν for the boundary-layer model with various values of the anisotropy parameter β_4. The solid curves have been computed by numerical integration of the nonlinear differential equation (4.1), and the dashed curves by numerical evaluation of the approximation (4.6). The heavy dots indicate values of ν at which the solvability condition is satisfied for the corresponding values of β_4.

APPENDIX: SOME MATHEMATICAL DETAILS

Asymptotic estimates for $\kappa'(0)$. To derive the asymptotic relation (3.16) for the geometrical model, we must evaluate integrals of the form

$$f_p(\nu)=\int_{-\infty}^{\infty} d\xi\,(\mathrm{sech}\xi)^p e^{i\xi/\sqrt{\nu}} \tag{A1}$$

in the limit $\nu\to 0$. This integration is most conveniently carried out by transforming to $\eta=\tan\theta$, where θ is the original angular variable that satisfies $\cos\theta=\mathrm{sech}\xi$. This technique is slightly more cumbersome than necessary for the geometrical model, but turns out to be specially suited for both the boundary-layer model to be considered next and the fully nonlocal problem.[11] In terms of η, we have

$$f_p(\nu)=\int_{-\infty}^{\infty} d\eta\,\frac{1}{(1+\eta^2)^{(1+p)/2}}\exp\left[\frac{i}{\sqrt{\nu}}\psi_G(\eta)\right], \tag{A2}$$

where

$$\psi_G(\eta)=\int_0^{\theta} d\theta'\,\frac{1}{\cos\theta'}=\int_0^{\eta} d\eta_1\,\frac{1}{(1+\eta_1^2)^{1/2}}\,. \tag{A3}$$

Inspection of (A2) and (A3) indicates that we should deform the contour of integration so as to pass near $\eta=i$ and then carry out a steepest-descent calculation in the neighborhood of that point. (The procedure in this case requires that the path of steepest-descent pass through the branch cut and back out again.) If $\eta=i+\omega$, $|\omega|\ll 1$, then

$$i\psi_G(\eta)=i\int_0^{i} d\eta_1\,\frac{1}{(1+\eta_1^2)^{1/2}}+i\int_0^{\omega} d\omega'\,\frac{1}{(2i\omega')^{1/2}}$$

$$\simeq-\frac{\pi}{2}+(2i\omega)^{1/2}\,, \tag{A4}$$

and

$$f_p(\nu)\approx\exp\left[-\frac{\pi}{2\sqrt{\nu}}\right]\int_{-\infty}^{\infty} d\omega\,\frac{1}{(2i\omega)^{(1+p)/2}}\exp\left[\frac{2i\omega}{\nu}\right]^{1/2}$$

$$=\frac{2\pi}{\nu^{(p-1)/2}\Gamma(p)}\exp\left[-\frac{\pi}{2\sqrt{\nu}}\right]. \tag{A5}$$

Note that, as mentioned previously, the dominant power of ν in the prefactor comes from the largest value of p; thus, in (3.16),

$$\kappa'(0)\approx-f_{7/2}(\nu)\,. \tag{A6}$$

The same technique works for the integral in (4.9), which we shall denote by $F_\mu(\nu)$. We have

$$F_\mu(\nu)=\int_{-\infty}^{\infty} d\eta\,\frac{1}{(1+\eta^2)^{(2\mu-3)/4}}\exp\left[\frac{i}{\sqrt{\nu}}\psi_B(\eta)\right], \tag{A7}$$

with

$$\psi_B(\eta)=\int_0^{\theta} d\theta'\,\frac{1}{(\cos\theta')^{7/2}}=\int_0^{\eta} d\eta_1(1+\eta_1^2)^{3/4}\,. \tag{A8}$$

Again, writing $\eta=i+\omega$ and integrating along the path of steepest descent through $\eta=i$, we find

$$F_\mu(\nu)\approx\exp\left[-\frac{a_s}{\sqrt{\nu}}\right]\int_{-\infty}^{\infty} d\omega\,\frac{1}{(2i\omega)^{(2\mu-3)/4}}$$

$$\times\exp\left[\frac{2}{7\sqrt{\nu}}(2i\omega)^{7/4}\right], \tag{A9}$$

which can be evaluated without further approximation to obtain the results shown in Eqs. (4.9)—(4.12).

Numerical methods. Numerical integrations of the nonlinear differential equations (2.5) and (4.1) were carried out with an implicit scheme using θ, κ, and $\lambda=d\kappa/d\xi$ as functions of arc length ξ. Initial conditions were computed using the asymptotic expansions as close to $\theta=\pi/2$ as possible, and then the equations were integrated back to $\theta=0$. Because, in practice, one can never start precisely on the trajectory which enters the fixed point, there will always be some components of the oscillating homogeneous solutions (3.3) in the function being computed. The frequency of the oscillation in (3.3) provides an estimate of the minimum step size $d\xi$ required to resolve these oscillations accurately. In addition, the rate at which the magnitudes of these homogeneous solutions decay in going toward $\theta=0$ from $\theta\simeq\pi/2$ provides an estimate of how accurately one must locate the correct trajectory near $\pi/2$ in order to obtain a desired accuracy of the

solution at $\theta=0$. These estimates were confirmed numerically (roughly) and were useful for achieving convergence of the numerical procedure.

Numerical evaluations of the various forms of the solvability formula (3.12), specifically (3.16) and (4.6), were performed using the trapezoidal rule with uniformly spaced intervals in ψ (as if performing a numerical Fourier transform). Results were extrapolated to $d\psi/\sqrt{\nu}\to 0$ and tested for convergence in the outer cutoff.

Note added in proof. The connection between singular perturbations and solvability conditions has been discussed by Barenblatt and Zel'dovich[12,13] in the general context of similarity solutions of partial differential equations. A recent development along these lines, closely related to the work described in the present paper, is the discovery of a solvability condition for pattern selection in the theory of viscous fingering. An excellent review of the latter topic has been prepared by Bensimon, Kadanoff, Liang, Shraiman, and Tang.[14] I am grateful to L. Kandanoff for informing me about Refs. 12 and 13 and for sending me a copy of Ref. 14 prior to publication.

ACKNOWLEDGMENTS

I should like to acknowledge especially useful conversations about mathematical aspects of this problem with M. Kruskal, C. Oberman, and H. Segur. This research was supported by the U.S. Department of Energy Grant No. DE-FG03-84ER45108, and also in part by the National Science Foundation Grant No. PHY-82-17853 supplemented by funds from the U.S. National Aeronautics and Space Administration.

[1]R. Brower, D. Kessler, J. Koplik, and H. Levine, Phys. Rev. Lett. 51, 1111 (1983); Phys. Rev. A 29, 1335 (1984).
[2]D. Kessler, J. Koplik, and H. Levine, Phys. Rev. A 30, 3161 (1984).
[3]E. Ben-Jacob, N. D. Goldenfeld, J. S. Langer, G. Schön, Phys. Rev. Lett. 51, 1930 (1983); Phys. Rev. A 29, 330 (1984).
[4]E. Ben-Jacob, N. D. Goldenfeld, B. G. Kotliar, and J. S. Langer, Phys. Rev. Lett. 53, 2110 (1984).
[5]J. S. Langer, Rev. Mod. Phys. 52, 1 (1980).
[6]G. P. Ivantsov, Dok. Akad. Nauk SSSR 58, 567 (1947).
[7]G. Horvay and J. W. Cahn, Acta Metall. 9, 695 (1961).
[8]M. Kruskal, C. Oberman, and H. Segur (private communication).
[9]D. Meiron (private communication).
[10]P. Pelcé and Y. Pomeau (unpublished).
[11]B. Caroli, C. Caroli, J. S. Langer, and B. Roulet, following paper, Phys. Rev. A 33, 442 (1986).
[12]G. I. Barenblatt and Ya. B. Zel'dovich, Annu. Rev. Fluid Mech. 4, 285 (1972).
[13]G. I. Barenblatt, *Similarity, Self-Similarity, and Intermediate Asymptotics* (Consultant's Bureau, New York, 1979).
[14]D. Bensimon, L. P. Kadanoff, S. Liang, B. I. Shraiman, and C. Tang (unpublished).

Development and evaluation of a multifunctional directly compressible diluent consisting of brittle and ductile materials.

Pharmaceutical Technology, Dec, 2003, by Mukesh C. Gohel, Laxman D. Patel, Shital H. Bariya, Rikita K. Dave, Nehal H. Bariya

The authors developed a coprocessed adjuvant consisting of microcrystalline cellulose, dibasic calcium phosphate dihydrate, and croscarmellose sodium. The properties of each component were evaluated and tablets of nimesulide were prepared to evaluate the functionalities of the coprocessed diluent. It was determined that the developed adjuvant exhibited satisfactory tableting characteristics.

****

Direct compression is widely used in tableting because it requires fewer processing steps, is simpler to validate, and improves drug stability when compared with the wet granulation method (1). Direct compression also eliminates exposure to heat and moisture during processing and is a more economical process. However, the majority of active pharmaceutical ingredients exhibit poor compressibility. Therefore, the addition of directly compressible adjuvants is mandatory in such cases.

A directly compressible filler-binder must exhibit good flowability and compactibility. Good flowability is necessary to ensure rapid and uniform die filling, whereas high compactibility is necessary to produce tablets having sufficient mechanical strength (2). No single diluent is likely to possess all the ideal characteristics. For this reason, the current trend in industry is to use multifunctional coprocessed adjuvants.

A survey conducted by Shangraw and Dermarest revealed that the most commonly used fillers for tablets and capsules are lactose, microcrystalline cellulose (MCC), starch, and dibasic calcium phosphate dihydrate (DCP) (3). MCC is well known as a tablet diluent, binder, and disintegrant. It is a ductile material that shows plastic deformation on compaction, which helps produce stronger tablets. However, MCC also is sensitive to hydrophobic lubricants and shows poor flowability, and therefore must be modified into large particles or agglomerates to improve its flow characteristics.

DCP has a high fragmentation propensity and therefore is insensitive to hydrophobic lubricants. It is also heat stable and has good flow properties (4). Other advantages of DCP are its low hygroscopicity and low cost. Sangekar et al. evaluated the performance of eight directly compressible excipients. Based on the results of hardness, change in disintegration time, moisture uptake, and change in volume, DCP was reported as the preferred directly compressible adjuvant (5). DCP is best used in direct compression when combined with MCC (6).

Several coprocessed filler-binders are commercially available, including Cellactose ([alpha]-lactose monohydrate and powdered cellulose 75:25), Microcelac ([alpha]-lactose monohydrate and powdered cellulose 75:25), Ludipress (93% [alpha]-lactose monohydrate, 3.5% polyvinylpyrrolidone, and 3.5% crospovidone), and Pharmatose DCL 40 (95% anhydrous [beta]-lactose and 5% lactitol) (7). The main objective of developing a coprocessed adjuvant is to obtain the advantages of each component in a single adjuvant. A combination of MCC, DCP, and croscarmellose sodium has not been fully explored either by industry or by researchers as a directly compressible multifunctional diluent. Therefore, in this investigation a coprocessed adjuvant consisting of the two diluents and croscarmellose sodium was developed.

Nearly all excipients for direct compression are manufactured by granulation, agglomeration, cocrystallization, or spray drying. Spray drying has been used commercially to manufacture excipients with good flowability and compressibility, but spray-dried products exhibit poor reworkability. Crystallization requires critical control of processing parameters. The method of wet granulation was adopted in this study because of its simplicity. The efficacy of the adjuvant was assessed by developing quick-disintegrating tablets of nimesulide.

Materials and methods

Materials. Nimesulide (100#) was received as a gift from Redson Pharmaceuticals Ltd. (Ahmedabad, India). MCC IP (MCC, 100#), starch, polyvinylpyrrolidone (PVP K30), hydroxypropyl methylcellulose (HPMC K15), and polyethylene glycol (PEG 4000) were received as gifts from Zydus Cadila Health Care Ltd.(Ahmedabad). DCP IP (DCP, 100#) was provided free of charge by Enar Chemie Pvt. Ltd. (Navsari, India). Croscarmellose sodium, sodium starch glycolate, and crospovidone were received as gift samples from Maruti Chemicals (Ahmedabad). Cab-O-Sil M5 was a gift from Cabot Sanmar Ltd. (Madras, India). Magnesium stearate (Vikas Pharma, Ahmedabad) and talc (JC Chemicals, Ahmedabad) were of IP grade.

Methods, Evaluation of binders. The premix of MCC and DCP (70:30, 50 g) was sieved and then remixed. The blend was granulated using

starch paste (Batch [A.sub.1], 10% w/v), PEG 4000 (Batch [A.sub.2], 26% w/w PEG 4000), PVP (Batch [A.sub.3, 10% w/v PVP), or HPMC (Batch [A.sub.4], 0.5% w/v HPMC) as a binder. A melt granulation technique was adopted for PEG 4000 and a wet-granulation technique was used for the rest of the binders. The liquid binder was mixed with the powder blend for 3 min and then the damp mass was warmed at 60 [degrees]C for 15-30 min in a hot-air oven to facilitate granulation. The wet coherent mass was then passed through a 44 mesh. The granules were dried at 60 [degrees]C for 90 min in a hot-air oven. The dried granules were again passed through a 44 screen. Fines were removed by shifting the granules on a 120 mesh. The granules were evaluated for angle of repose and Carr's index. Talc (2%) and magnesium stearate (1%) were mixed with the granules, and tablets with an average weight of 220 mg were prepared on a single-punch tablet machine (Cadmach Machinery Ltd., Ahmedabad). Tablets were evaluated for crushing strength and disintegration and the results are shown in Table I.

Angle of repose. Angle of repose was measured using the fixed-funnel method with a reposograph (model 640, Enar Foundation Research Center, Navsari) (8). Per the manufacturer's instruction, the samples were graded as excellent, good, fair, or meager if the angle of repose was found to be in the range of 30-32[degrees], 32-35[degrees], 35-37[degrees], or 37-45[degrees], respectively.

Bulk density and tapped density. The granules were filled in a 100-mL capacity measuring cylinder up to the 75-mL mark. Bulk density is the quotient of weight to the volume of a sample. Tapped density is the quotient of weight of a sample to its volume after tapping the measuring cylinder 500 times at a height of ~1.5 in.

Carr's index. The percentage compressibility (Carr's index) was calculated as 100 times the ratio of the difference between tapped density and bulk density to the tapped density (9).

Crashing strength. The crushing strength of the tablets was determined after 24 h of compression (time for stress relaxation) using a Monsanto hardness tester (Shital Scientific Industries, Mumbai, India).

Friability. Friability was evaluated from percentage weight loss of 20 tablets tumbled in a friabilator (model EF2, Electrolab, Mumbai) at 25 rpm for 4 min. The tablets then were dedusted, and the loss in weight caused by fracture or abrasion was recorded as percentage weight loss.

Disintegration time. The time required for disintegration of six tablets placed in the tubes of a disintegration test apparatus (model ED2, Electrolab, Mumbai) was measured at 37 [+ or -] 2 [degrees]C using 900 mL distilled water (10).

Evaluation of superdisintegrants. Croscarmellose sodium (CCS), sodium starch glycolate (SSG) and crospovidone (CRP) were tried as superdisintegrants at a level of 4%. Granules were prepared using starch paste (10% w/v) and were compressed on a single-punch tablet machine. Each tablet was evaluated for disintegration in a petri dish (diameter = 5.5 cm). A tablet was placed carefully in the center of a petri dish containing 20 mL of water. The tablet was allowed to wet for 30 s and then the petri dish was subjected to 10 oscillations of one inch each. Particle-size measurements were performed using a microscopic method after decanting the clear liquid. The results are shown in Figure 1.

Preparation of physical blend of MCC and colloidal silicon dioxide. A physical blend of 97% MCC and 3% colloidal silicon dioxide was prepared by blending them in a glass mortar for 30 min. The silica-treated MCC (35 g), DCP (15 g), and croscarmellose sodium (2 g) were blended subsequently. The granules of 44/120 # were prepared using starch paste (10% w/v) as a binder and then were evaluated for angle of repose and Carr's index. Tablets containing silica-treated MCC and untreated MCC were separately prepared and compared (see Table II, Batch B).

Lubricant sensitivity test. The effect of magnesium stearate on the crushing strength and the disintegration of tablets containing treated MCC as well as untreated MCC were studied (batches [C.sub.1]-[C.sub.4]). Magnesium stearate (1%) was mixed with the granules for 2 min in a glass jar. The granules ready for compression were compressed into tablets and the tablets were evaluated for crushing strength and disintegration. Table III shows the results of the lubricant sensitivity test.

1 · 2 · 3 | Next »

RELATED TERMS

- Pharmaceutical industry Production processes